Supporting Information: Water Flow in Graphene Nanochannels Driven by Imposed Thermal Gradients: The Role of Flexural Phonons

Elton Oyarzua,[†] Jens H. Walther,[‡,¶] and Harvey A. Zambrano[*,§]

[†]*Department of Computing Technologies, Swinburne University of Technology, P.O. Box 218 Hawthorn, Victoria 3122, Australia*

[‡]*Department of Mechanical Engineering, Technical University of Denmark, DK-2800 Kgs. Lyngby, Denmark*

[¶]*Computational Science and Engineering Laboratory, Department of Mechanical and Process Engineering, ETH Zurich, CH-8092 Zurich, Switzerland*

[§]*Department of Mechanical Engineering, Universidad Técnica Federico Santa María, Valparaiso, Chile*

E-mail: harvey.zambrano@usm.cl

Phone: +56 (0)41 2201468

Dimensions, Details and Operation of the Thermal Pump

The thermal water-pump studied in this research consists of two parallel graphene layers separated by 2 nm (Figure S1a) completely filled with water. Each graphene layer consists of 7200 carbon atoms with a total axial length of 50 nm in the armchair direction. From it, 360 carbon atoms are used as heaters at each end, depicted by the colors red (high temper-

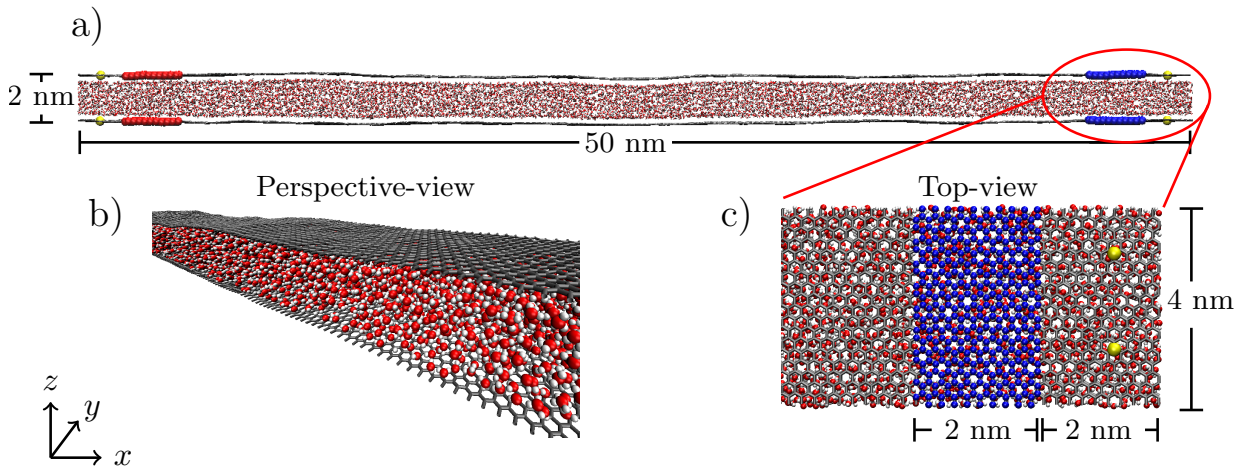

Figure S1: Schematic representation of the thermal water-pump analyzed in this research. The graphene layers are restricted in motion by fixing carbon atoms at 1 nm from the boundary of the computational box (yellow atoms). The red atoms depict the high temperature carbon atoms and the blue atoms the low temperature carbon atoms. a) Nanochannel heated at both sides (above and below). b) Perspective representation of the nanochannel. c) Top-view at the right end of the nanochannel depicting the fixed carbon atoms (yellow dots) and the low-temperature heated carbon atoms.

ature) and blue (low temperature), with an approximate length of 2 nm (see Figure S1c). Additionally, the heated carbon atoms are located from 2 nm of the boundary of the computational box. Two carbon atoms are frozen (position and momentum not updated) at each end of the graphene layers in order to restrict the mean position of the layers and also emulate the end supports of the graphene channel (see Figure S1c). These carbon atoms are located at 1 nm approximately from the boundary of the computational box. A total of 10060 water molecules are used to fill the nanonchannel ensuring a pressure of 1 bar inside the nanochannel by following the procedure of Wagemann et al.[S1]

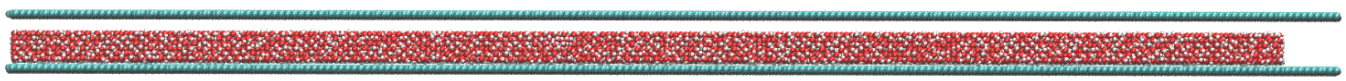

Figure S2: Screenshot of the initial configuration.

The equilibration and preparation of the system is described in the following. The initial

configuration was prepared using a separation distance of 2 nm between the layers with a total length of the channel of 50 nm. A screenshot of the initial configuration is presented in Figure S2. The number of molecules of 10060 is taken from the work of Wagemann et al.[S1] for the channel with a 2 nm height, extrapolated for a total surface area of ∼200 nm^2. After an equilibration of the water molecules at 300 K, the procedure of Wagemann et al.[S1] was implemented to ensure an internal pressure of 1 bar. This technique consists on applying a force to the carbon atoms at the bottom graphene layer in the positive "z" direction, mimicking a piston with a target pressure of 1 bar. After equilibration, two carbon atoms at the respective ends are frozen to keep the channel height with an approximated average value of 2 nm. It is important to recall that a specific time-frame has to be chosen to froze the aforementioned fixed points. The one that showed and average height closer to 2 nm was chosen. A plot including the dimensions of the system is depicted in Figure S3 after the 300 K and 1 bar equilibration, showing the corrugation of graphene and the average height distance of 2 nm.

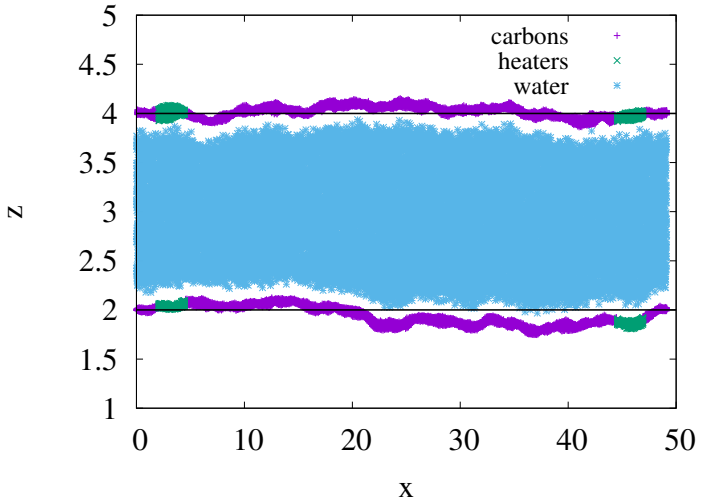

Figure S3: Data plot depicting the position of the particles after equilibration of 300 K and 1 bar.

The operation of the proposed thermal-pump can be understood as a chain of repeated device units of graphene nanochannels as depicted in Figure S4, similar to the works of

Oyarzua et at.[S2] and Leng et al.[S3]. Thanks to periodic boundary conditions, the water molecules leaving the computational box at the right end of the channel, reenters at the left end of the channel, or vice-versa, simulating the scheme presented in Figure S4. Thus, considering that the behavior of the central unit is replicated on the specular images thanks to periodicity, the conclusions obtained of phonons and lattice dynamics from the central section are valid for all the units.

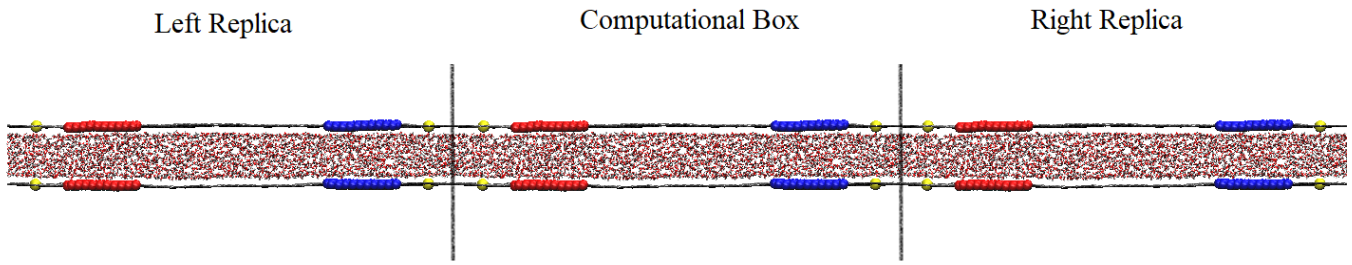

Figure S4: Schematic representation of the axial periodicity of the thermal pump.

Temperature Profiles

The different temperatures imposed at the ends of the graphene layers induce different axial temperature profiles along the graphene layer. The temperature profiles along the graphene for temperatures of 400 K–300 K, 375 K–300 K and 350 K–300 K are depicted in Figure S5. Notice that the temperature distributions display non-linear profiles indicating non-Fourier heat conduction in the graphene layers in line with previous investigations[S4–S6]. Therefore, in order to quantify the thermal gradients imposed in our system, a linear fit is performed in the central zone of the temperature profile, depicted by the dashed lines in Figure S5. For imposed temperatures of 400 K–300 K a thermal gradient of 0.8 K/nm is computed in the central zone, for temperatures of 375 K–300 K a thermal gradient of 0.6 K/nm is computed while for temperatures of 350 K–300 K a thermal gradient of 0.4 K/nm is computed.

By imposing a thermal gradient in the graphene layers, a slight axial temperature gradient is also induced in the confined water. The axial temperature profiles of graphene and water

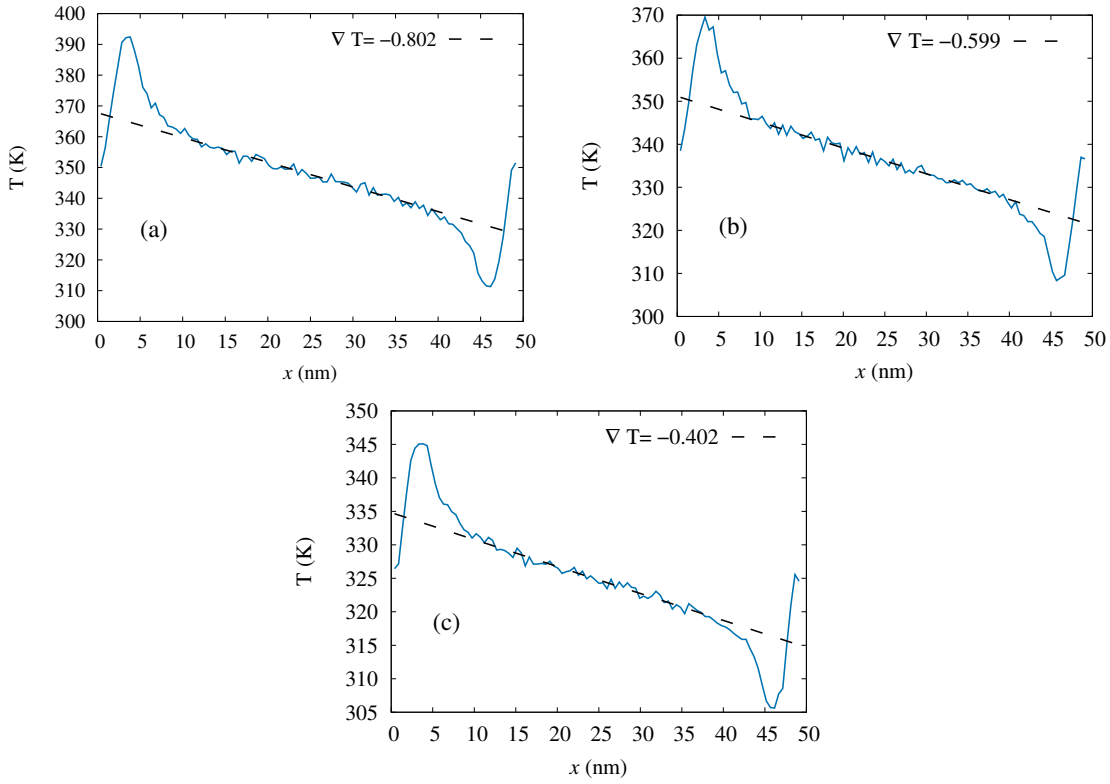

Figure S5: Temperature profiles along the 50 nm-long graphene layer for imposed temperatures of a) 400 K–300 K b) 375 K–300 K and c) 350 K–300 K. The blue line (—) is the temperature profile of the top graphene layer. The dashed black lines (—) is a linear fit at the central zone of the graphene layer.

for the case with imposed temperatures of 400 K–300 K (highest imposed thermal gradient) are depicted in Figure S6. In this case, a temperature difference of 15 K is computed from the peaks of the water temperature profile.

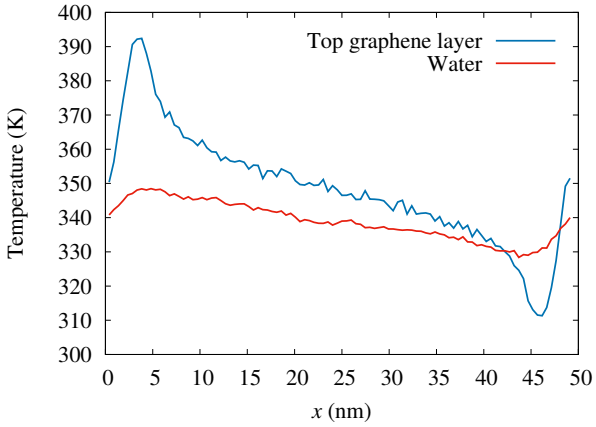

Figure S6: Temperature profile comparison between the top graphene layer and the water molecules confined in the nanochannel in the axial direction. The applied temperatures are 400 K–300 K.

Mean water flow comparison between the proposed thermal pump configurations

In this section, the magnitudes of the water flows produced in the thermal pump concepts of Figure 1a and Figure 1b of the main article are compared side-by-side. By applying the same temperature differences of 350 K–300 K, 375 K–300 K and 400 K–300 K in both thermal pump concepts, higher water flows are computed in the case with two layers heated (Figure 1a case) in comparison to the case with a single layer heated (Figure 1b case). Indeed, as depicted in Figure S7, at each imposed thermal gradient, lower flow rates are computed in the case with a single heated layer (Figure 1b case). In Figure S7 the dashed lines correspond to linear fits under the condition of $v_{(\Delta T=0)} = 0\,\mathrm{m/s}$.

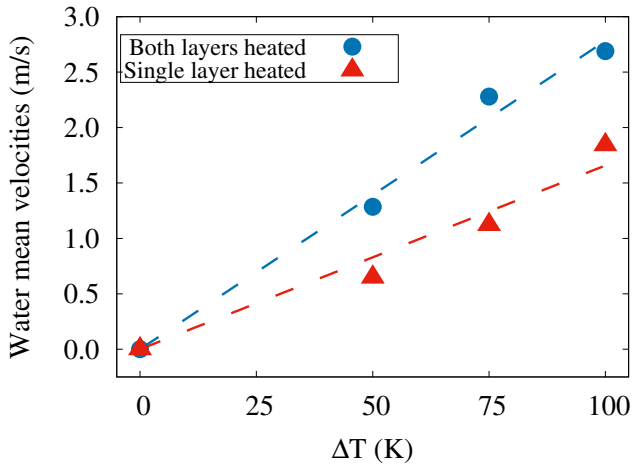

Figure S7: Mean water flows produced in both thermal pump configurations presented in Figure 1 of the main article. The thermal pump configuration with both layers heated is depicted in Figure 1a of the main article and the thermal pump with a single layer heated is represented in Figure 1b of the main article. The dashed lines correspond to linear fits under the condition of $v_{(\Delta T=0)} = 0\,\mathrm{m/s}$.

Restrained simulations

In order to evaluate the influence of the out-of-plane flexural phonons of the graphene layer in the operation of our thermal pump, the out-of-plane motion dynamics of the graphene layer is restricted in the device by imposing an external potential on each graphene layer. To achieve this, external ghost-layers are introduced above and below of each graphene layer as depicted in Figure S8. These ghost-layers are frozen graphene layers (position and momentum not updated) interacting only with the thermalized graphene layers by means of interatomic potentials, not to the water molecules. A separation distance of 0.34 nm is chosen between the graphene layers, based on the interlayer spacing of graphite.[S7,S8]

In this analysis, two interatomic potentials are used to restrict the out-of-plane motion dynamic of the graphene layers, a repulsive Buckingham interatomic potential and a Lennard-Jones potential.

The Buckingham potential has the form,

$$V_B = a_{ij} \exp\left(-b_{ij} r_{ij}\right) - \frac{c_{ij}}{r_{ij}^6}$$

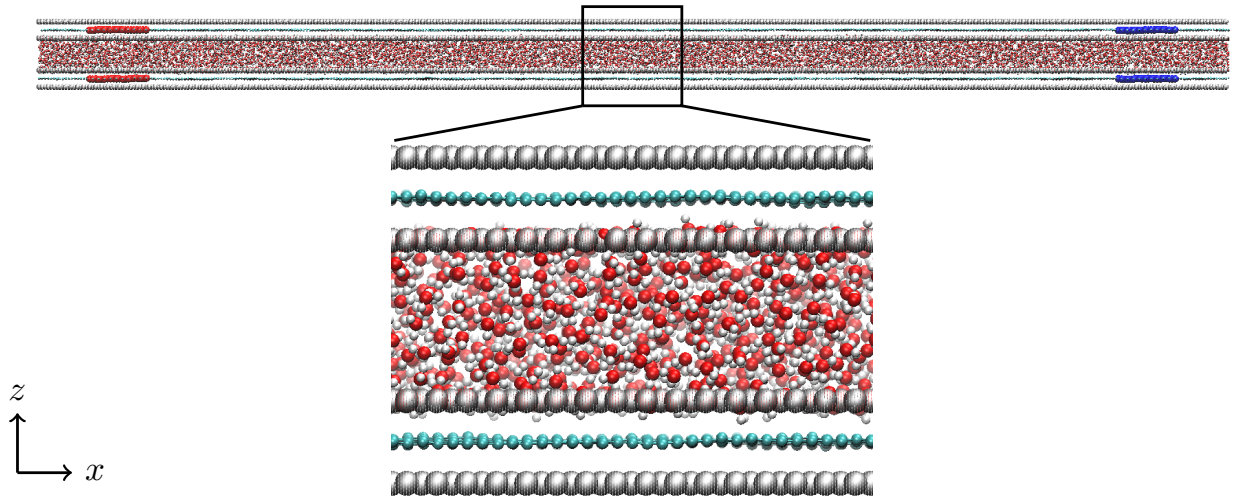

Figure S8: Schematic of the thermal pump with external layers to restrain the out-of-plane motion of the graphene layers. The cyan atoms depict the carbons in the graphene layers and the gray atoms depict the atoms in the ghost layers.

and by neglecting the attractive term ($c_{ij} = 0$), we are imposing a repulsive potential to the graphene layers from above and below. In the first attempt to impose the repulsive potential we use a slight repulsive interatomic potential based on the Water-hydrogen/Silica interaction with the parameters of $a_{ij} = 6830.682$ kJ/mol and $b_{ij} = 32.65839$ nm[S9] . For the Lennard-Jones potential we use the interatomic C-C Lennard Jones potential from the UFF, with the parameters of $\epsilon_{CC} = 0.4396\,\text{kJ/mol}$ and $\sigma_{CC} = 0.3851\,\text{nm}$. As shown in Figure 3a of the main article, the flexural restriction with a LJ potential greatly reduces the water flow produced in the thermal pump. Moreover, the temperature profile of the graphene layers is not affected by the imposed restriction (See Figure 3b of the main article).

Analysis of the lattice dynamics of the heated graphene layer.

The analysis of the lattice dynamics is presented in Figure S9 by following the procedure of Dickey & Pask[S10] and Zhang et al.[S11] First, the velocity correlation function is computed according to,

$$\gamma(t) = \frac{\langle \sum v_i(t) \cdot v_i(0) \rangle}{\langle \sum v_i^2(0) \rangle}$$

Subsequently, with the extracted signal of the velocity correlation function, a Fast Fourier Transform (FFT) is applied to the data. As an example, the velocity correlation function for the out-of-plane dynamics of the graphene layer is depicted in Figure S9a (z-component of the velocity) and the FFT of that signal is shown in Figure S9b. Thereafter, a Gaussian smearing is implemented in the FFT signal in order to obtain a smoother signal. In this example, a bandwidth of 0.8 THz is applied to the signal in Figure S9c and a bandwidth of 1.2 THz is applied to the signal in Figure S9d. It is important to note that the velocity correlation function is computed only in the non-heated carbon atoms in order to avoid any spurious effect in the analysis due to the thermostat. In the main article, a Gaussian smearing width of 0.8 THz is implemented to compare and analyze the phonon-dispersion curves.

The phonon dynamics is decomposed into in-plane, out-of-plane and total DOS by computing the FFT of the velocity correlation function with the corresponding velocity components separately.[S11,S12] In the case with imposed temperatures of 400 K–300 K, the phonon density spectra of the graphene layer for the in-plane, out-of-plane and total DOS is presented in Figure S10. Different representations of the same data are presented in order to better visualize the dynamic behavior. It is important to note that the phonon DOS presented here are in good agreement with the work of Zhang et al.[S11]

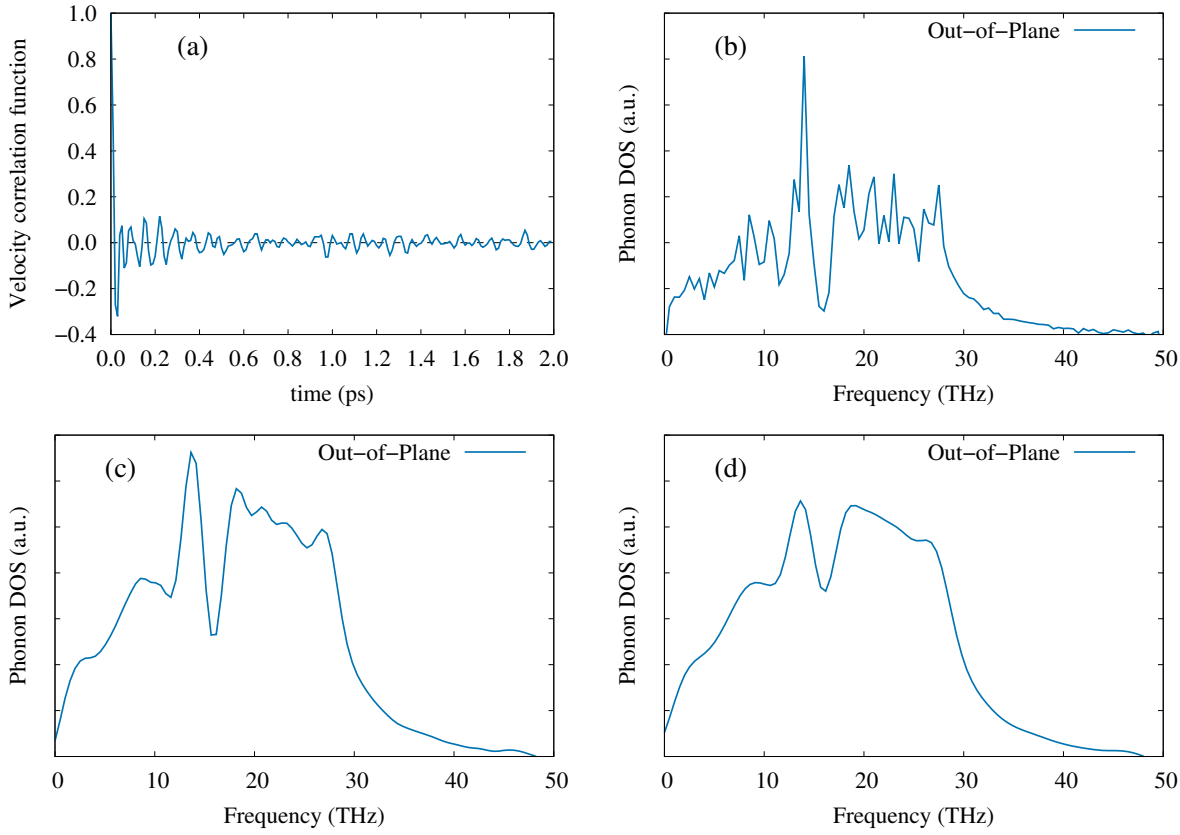

Figure S9: Lattice dynamics analysis of the heated graphene layer in the case with imposed temperatures of 400 K–300 K. a) Velocity correlation function of the out-of-plane velocity component (v_z). b) FFT of the velocity correlation function in Figure a). c) Smoothed FFT signal with a Gaussian smearing width of 0.8 THz. d) Smoothed FFT signal with a Gaussian smearing width of 1.2 THz.

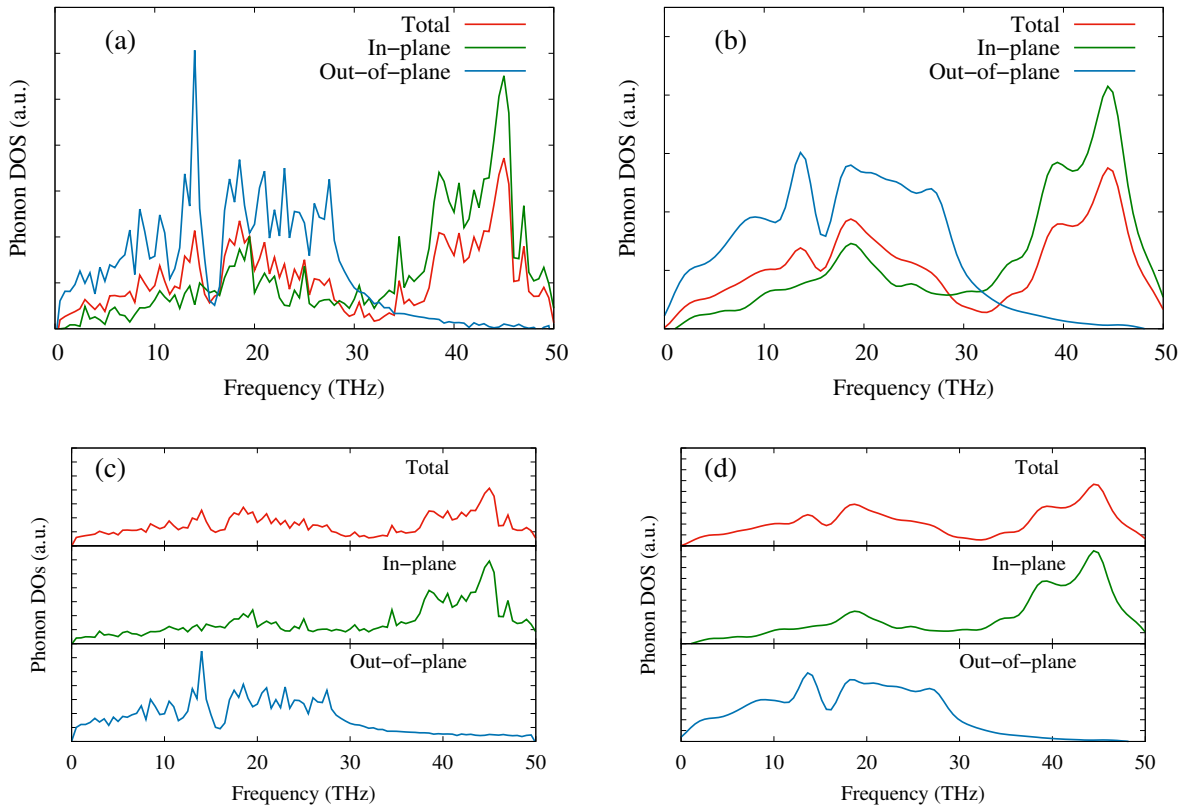

Figure S10: Phonon-dispersion curves of the heated graphene layer for the case of 400 K–300 K for in-plane dynamics, out-of-plane dynamics, and total dynamics. a) and c) Different representations of the spectra. b) and d) Smoothed signal of Figure a) and c) respectively with a bandwidth smearing of 1.0 THz.

Zoom-in of the broadening of out-of-plane DOS.

In Figure S11 we present a close-up of Figure 5b of the main article, between frequencies 4 and 12 THz. Figure S11 clearly shows the systematic broadening of the dispersion curves with lower frequency peaks at higher thermal gradients, similar to a "traveling wave" moving from the lowest thermal gradient (solid black line) to the highest thermal gradient (solid blue line).

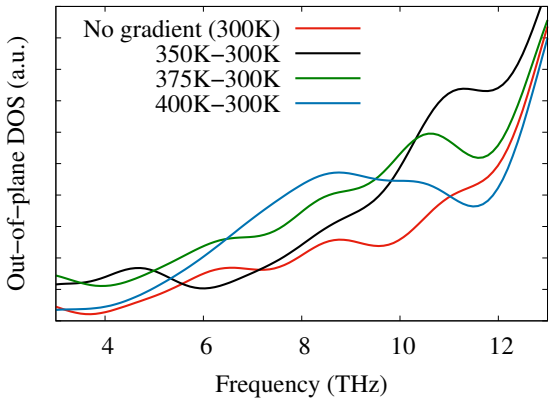

Figure S11: Out-of-plane DOS (ZA) of the heated graphene layer for the system shown in Figure 1b (top layer) of the main article. This plot is close-up of Figure 5b of the main article between frequencies 4 and 12 THz. The applied temperatures are 350 K–300 K, 375 K–300 K and 400 K–300 K. The phonon DOS with no imposed thermal gradient is also included.

Axial distribution of the water flow velocity.

In the main article we presented the water axial velocity profiles considering a height distribution (see Fig.3a and Fig. 7b of the main article), where a flat profile through the channel cross-section is observed on average for all the systems and cases investigated. However, by analyzing the water flow velocity considering an axial distribution (variation of the velocity in the x-direction) some differences in magnitude are observed. In Figure S12a the axial distribution of the water flow velocity for the case with the lowest applied thermal gradient (applied temperatures of 350 K–300 K) is shown. In this case, the water flow velocity has a constant value of 1.4 m/s on average along the entire channel in the x-direction. Furthermore, in Figure S12b the axial distribution of the water flow velocity for the case with the highest applied thermal gradient (applied temperatures of 400 K–300 K) is shown. Here, unlike the case with temperatures of 350 K–300 K, a difference of 0.5 m/s in the flow velocity is observed between the regions with the high and the low temperatures imposed. In fact, for the case with the highest applied thermal gradient, the water flow velocity displays a slight increase in magnitude in the high temperature zone i.e., the region including the heater with the higher applied temperature (400 K). This result indicates that most of the boost of the water flow is gained from the high temperature zone in the proposed thermal-pump.

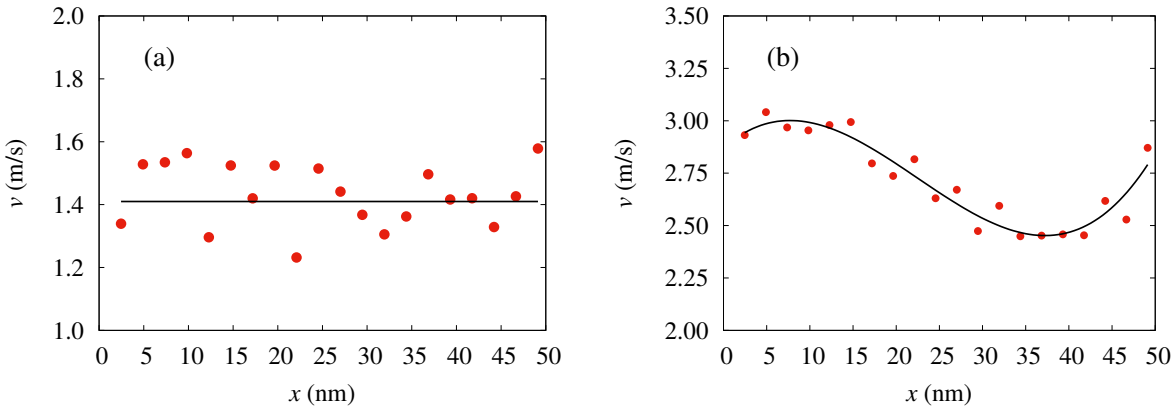

Figure S12: Axial distribution of the water flow for the system shown in Figure 1a (both layers heated). The applied temperatures correspond to a) 350 K–300 K and b) 400 K–300 K.

Diffusivity of water.

In order to discuss the diffusion mechanisms of the water molecules confined in the nanochannel, the mean-square-displacement (MSD) of the water molecules is computed according to,

$$\mathrm{MSD} = \left\langle |\mathbf{r}(t) - \mathbf{r}(0)|^2 \right\rangle \tag{1}$$

where the different mechanisms can be described using the next expression,

$$\mathrm{MSD} = 2dDt^n \tag{2}$$

where d stands for the dimensionality of the system, D the diffusion constant and n describing the diffusion mechanism, with $n = 0.5$ referring to single-file diffusion, $n = 1$ the Fickian diffusion, and $n = 2$ referring to ballistic diffusion. The analysis performed here are based on the work of Barati et al.[S13], Marti et al.,[S14] Zaragoza et al.[S15] and Zhao et al.[S16] for nanoconfined fluids. Here, the comparison of diffusivity of water between the LJ-restrained case with a ΔT of 400 K-300 K (Figure 6 in the main paper) and the isothermal case at 300 K is performed.

In Figure S13a the MSD for the isothermal case at 300 K is shown. The MSD using the real positions of particles is depicted by the blue line (MSD_{xyz}), the MSD computed by removing the center-of-mass of the fluid system is represented by the green line (MSD_{xyz}com), the two-dimensional (2D) MSD using the real positions of particles in the xy-coordinate is depicted by red (MSD_{xy}) and the 2D-MSD by removing the center of mass of the fluid is in yellow (MSD_{xy}com). From the figure, we clearly observe that the MSD is the same for the four methods analyzed, showing that the xy diffusion is the dominant direction of diffusivity, as expected for a 2D system. It is important to mention that by removing the center-of-mass positions the MSD is reduced only slightly, its contribution being negligible considering that the diffusion analysis is based on the slope behavior of MSD.

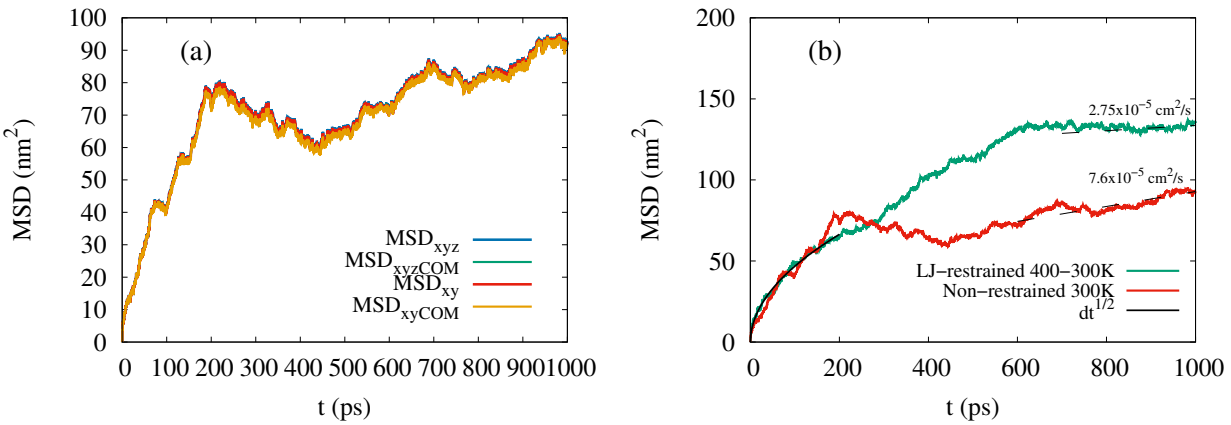

Figure S13: Diffusion enhancement due to graphene wiggling of water in the nanochannel. a) MSD of the isothermal case at 300 K. The 3D-MSD is depicted in blue, the 3D-MSD with subtracted center-of-mass of the fluid is in green, the 2D-MSD is in red, and the 2D-MSD with removed center-of-mass is in yellow. b) MSD$_{xyz}$ comparison between the LJ-restrained case with applied temperatures of 400 K-300 K and the non-restrained isothermal case at 300 K with the corresponding diffusion coefficients.

The MSD comparison between the LJ-restrained case and the non-restrained isothermal case at 300 K is presented in Figure S13b. Here, at 1000 ps, the LJ-restrained case shows a diffusion constant of water of 2.75×10^{-5} cm^2/s and the non-restrained isothermal case shows a diffusion constant of 7.6×10^{-5} cm^2/s. By comparing these results with the bulk diffusion constant for SPC/E water ($D = 2.59 \times 10^{-5}$ cm^2/s[S13]) we observe that the LJ-restrained case at 1000 ps shows only a slight increase of 6% in the diffusion constant, indicating that the confined water molecules experience almost no diffusion enhancement coming from the graphene wiggling. On the other hand, the non-restrained isothermal case shows a 3 times enhancement of diffusion compared to the bulk value, exhibiting the enhancement of diffusion due to the wiggling of graphene, in line with Ma et al.[S17] and Marbach et al.[S18]

Although this result unveils a key aspect of the diffusion mechanisms in the proposed thermal pump, we believe that a complete analysis of the fluid behavior and diffusivity of water in the proposed thermal-pump is further needed and must be performed extensively in the near future. The analysis of the diffusion mechanisms of water in nanochannels have several approaches. First, the diffusion of water relies on the level of confinement of

the system, where it has been observed a dependency of the diffusion with respect to the height of the nanochannel[S14,S16,S19]. Secondly, graphene as a confining wall modifies the diffusivity of water due to its large hydrodynamic slippage with water and to its intrinsic corrugation[S17], where active (or frozen[S16]) graphene plays an important role trough friction. Additionally, the spatial behavior of water diffusion is also important, where it has been observed in carbon nanotubes[S13], that confined water molecules near the solid experience a diffusion enhancement compared to the central zone. Finally, it should be noted that the non-equilibrium thermal state of our system adds an additional level of complexity that makes the analysis of the aforementioned points even more challenging.

Tangential van der Waals Force.

In this section, the methodology proposed by Leng et al.[S3] and Zhu et al.[S20] to compute the driving force of thermal-water-pumps is presented. This method consists on computing the tangential van der Waals (vdW) force (axial force in the x-direction) of the atoms in the solid acting on the water molecules along the nanochannel. Considering that our system does not have junctions or changes in cross sections, we can analyze the total channel as a single volume. Additionally, in order to store the specific vdW interaction, the molecular dynamics code must be modified accordingly. The pseudo-code of this computation for a single time-step is presented below.

```
!-------------------------------------------------------------------------------
! pseudo code of the vdW forces acting on water for a single time step
!-------------------------------------------------------------------------------
 IF (func.EQ.LJ_6_12) THEN
    IF ((atom_i.EQ.O.OR.atom_i.EQ.H).AND.(atom_j.EQ.C.OR.&
    &     atom_j.EQ.C_Hot.OR.atom_j.EQ.C_Low)) THEN
            vdwF(1) = vdwF(1) + 1
            vdWF(2) = vdwF(2) - fx ! tangential force
    ELSEIF ((atom_j.EQ.O.OR.atom_j.EQ.H).AND.(atom_i.EQ.C.OR.&
    &         atom_i.EQ.C_Hot.OR.atom_i.EQ.C_Low)) THEN
            vdwF(1) = vdwF(1) + 1
            vdwF(2) = vdwF(2) + fx ! tangential force
    ENDIF
 ENDIF
```

We averaged these forces for a total simulation time of 5 ns with applied temperatures of 350 K-300 K, 375 K-300 K and 400 K-300 K. The mean force magnitudes obtained at each temperature difference are reported in Figure S14. Our results show that the average vdW forces obtained for all the imposed temperature differences point towards the colder temper-

ature region along the graphene channel, therefore in the same direction of the produced net water flow.

Although this result shows no alteration of the tangential vdW force with respect the applied temperature difference, we believe that the out-of-plane phonons and the vdW forces of graphene acting on water are linked and both should give related answers for the generation of fluid motion in thermal-water-pumps. Therefore, we think that the methodology proposed by Leng et al.[S3] and Zhu et al.[S20] is the starting point to address the mechanical force that drives the motion in graphene/water systems, however, further theoretical and computational analysis[S20] must be conducted for graphene/water in order to reach a comprehensive understanding of the forces contributing to the production of flow including the role of friction. A related investigation was proposed by our group[S21], wherein the total thermophoretic force acting on water nanodroplets confined in a single-walled CNT was computed from molecular dynamics simulations. This force was measured by subtracting the friction force to the total net force acting on the droplet at the corresponding velocities.

In summary, we believe that a study that address the mechanical force that drives the flow in graphene/water thermal-pump systems must be performed extensively, addressing all the variables affecting this system such as the intrinsic high slip in graphene/water systems, the anharmonic corrugation of the solid, the rippling dependency with temperature, the enhanced diffusion of water, the contact surface dependency and the height of the channel, to mention a few.

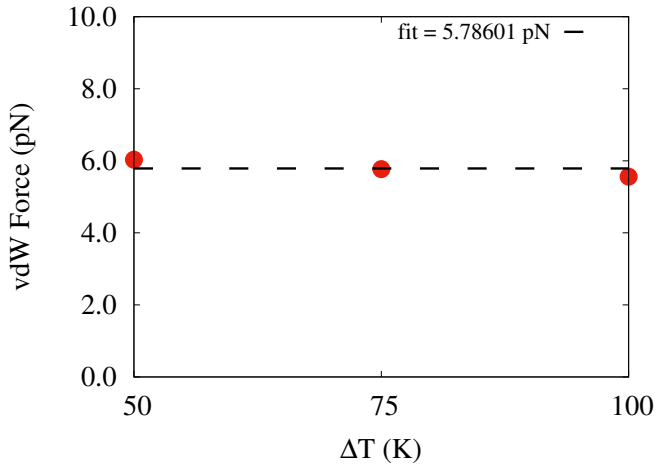

Figure S14: Axial van der Waals force of carbons acting on the water molecules at three temperature differences.

References

(S1) Wagemann, E.; Oyarzua, E.; Walther, J. H.; Zambrano, H. A. Slip Divergence of Water Flow in Graphene Nanochannels: The Role of Chirality. *Phys. Chem. Chem. Phys.* **2017**, *19*, 8646–8652.

(S2) Oyarzua, E.; Walther, J. H.; Megaridis, C. M.; Koumoutsakos, P.; Zambrano, H. A. Carbon nanotubes as thermally induced water pumps. *ACS nano* **2017**, *11*, 9997–10002.

(S3) Leng, J.; Ying, T.; Guo, Z.; Zhang, Y.; Chang, T.; Guo, W.; Gao, H. Thermally induced continuous water flow in long nanotube channels. *Carbon* **2022**, *191*, 175–182.

(S4) Yao, W.-J.; Cao, B.-Y. Thermal Wave Propagation in Graphene Studied by Molecular Dynamics Simulations. *Chin. Sci. Bull.* **2014**, *59*, 3495–3503.

(S5) Rajegowda, R.; Kannam, S. K.; Hartkamp, R.; Sathian, S. P. Thermophoretically Driven Water Droplets on Graphene and Boron Nitride Surfaces. *Nanotechnol.* **2018**, *29*, 215401.

(S6) Xu, M. Nonlocal heat conduction in suspended graphene. *Phys. Lett. A* **2019**, *383*, 1–5.

(S7) Hod, O. Graphite and Hexagonal Boron-Nitride Have the Same Interlayer Distance. Why? *J. Chem. Theory Comput.* **2012**, *8*, 1360–1369.

(S8) Chung, D. Review Graphite. *J. Mater. Sci.* **2002**, *37*, 1475–1489.

(S9) Zambrano, H. A.; Walther, J. H.; Jaffe, R. L. Molecular Dynamics Simulations of Water on a Hydrophilic Silica Surface at High Air Pressures. *J. Mol. Liq.* **2014**, –, In Press.

(S10) Dickey, J.; Paskin, A. Computer Simulation of The Lattice Dynamics of Solids. *Phys. Rev.* **1969**, *188*, 1407.

(S11) Zhang, H.; Lee, G.; Cho, K. Thermal Transport in Graphene and Effects of Vacancy Defects. *Phys. Rev. B* **2011**, *84*, 115460.

(S12) Luo, T.; Lloyd, J. R. Enhancement of Thermal Energy Transport Across Graphene/-Graphite and Polymer Interfaces: A Molecular Dynamics Study. *Adv. Funct. Mater.* **2012**, *22*, 2495–2502.

(S13) Barati Farimani, A.; Aluru, N. R. Spatial diffusion of water in carbon nanotubes: from fickian to ballistic motion. *J. Phys. Chem. B* **2011**, *115*, 12145–12149.

(S14) Marti, J.; Nagy, G.; Guardia, E.; Gordillo, M. Molecular dynamics simulation of liquid water confined inside graphite channels: dielectric and dynamical properties. *J. Phys. Chem. B* **2006**, *110*, 23987–23994.

(S15) Zaragoza, A.; González, M. A.; Joly, L.; López-Montero, I.; Canales, M.; Benavides, A.; Valeriani, C. Molecular dynamics study of nanoconfined TIP4P/2005 water: how confinement and temperature affect diffusion and viscosity. *Phys. Chem. Chem. Phys.* **2019**, *21*, 13653–13667.

(S16) Zhao, Z.; Zhou, R.; Sun, C. Molecular dynamics study of water diffusivity in graphene nanochannels. *Internat. J. Thermophys.* **2020**, *41*, 1–12.

(S17) Ma, M.; Tocci, G.; Michaelides, A.; Aeppli, G. Fast diffusion of water nanodroplets on graphene. *Nature Mat.* **2016**, *15*, 66–71.

(S18) Marbach, S.; Dean, D. S.; Bocquet, L. Transport and Dispersion Across Wiggling Nanopores. *Nature Physics* **2018**, *14*, 1108.

(S19) Simonnin, P.; Noetinger, B.; Nieto-Draghi, C.; Marry, V.; Rotenberg, B. Diffusion under confinement: Hydrodynamic finite-size effects in simulation. *J. Chem. Theory Comput.* **2017**, *13*, 2881–2889.

(S20) Zhu, F.; Leng, J.; Jiang, J.-W.; Chang, T.; Zhang, T.; Gao, H. Thermal-fluctuation gradient induced tangential entropic forces in layered two-dimensional materials. *J. Mech. Phys. Solids* **2022**, *163*, 104871.

(S21) Oyarzua, E.; Walther, J. H.; Zambrano, H. A. Water thermophoresis in carbon nanotubes: the interplay between thermophoretic and friction forces. *Phys. Chem. Chem. Phys.* **2018**, *20*, 3672–3677.